THE UNIVERSITY of EDINBURGH

Edinburgh Research Explorer

Inverting for emissions of carbon monoxide from Asia using aircraft observations over the western Pacific

OPEN ACCESS

Inverting for emissions of carbon monoxide from Asia using aircraft observations over the western Pacific

Paul I. Palmer, Daniel J. Jacob, Dylan B. A. Jones, Colette L. Heald, Robert M. Yantosca, and Jennifer A. Logan

Division of Engineering and Applied Sciences, Harvard University, Cambridge, Massachusetts, USA

Glen W. Sachse

NASA Langley Research Center, Hampton, Virginia, USA

David G. Streets

Argonne National Laboratory, Argonne, Illinois, USA

[1]   We use aircraft observations of continental outflow over the western Pacific from the Transport and Chemical Evolution over the Pacific (TRACE-P) mission (March–April 2001), in combination with an optimal estimation inverse model, to improve emission estimates of carbon monoxide (CO) from Asia. A priori emissions and their errors are from a customized bottom-up Asian emission inventory for the TRACE-P period. The global three-dimensional GEOS-CHEM chemical transport model (CTM) is used as the forward model. The CTM transport error (20–30% of the CO concentration) is quantified from statistics of the difference between the aircraft observations of CO and the forward model results with a priori emissions, after removing the mean bias which is attributed to errors in the a priori emissions. Additional contributions to the error budget in the inverse analysis include the representation error (typically 5% of the CO concentration) and the measurement accuracy ($\simeq$2% of the CO concentration). We find that the inverse model can usefully constrain five sources: Chinese fuel consumption, Chinese biomass burning, total emissions from Korea and Japan, total emissions from Southeast Asia, and the ensemble of all other sources. The inversion indicates a 54% increase in anthropogenic emissions from China (to 168 Tg CO yr^{-1}) relative to the a priori; this value is still much lower than had been derived in previous inversions using the CMDL network of surface observations. A posteriori emissions of biomass burning in Southeast Asia and China are much lower than a priori estimates.   *INDEX TERMS:* 0322 Atmospheric Composition and Structure: Constituent sources and sinks; 0345 Atmospheric Composition and Structure: Pollution—urban and regional (0305); 0365 Atmospheric Composition and Structure: Troposphere—composition and chemistry; 0368 Atmospheric Composition and Structure: Troposphere—constituent transport and chemistry; *KEYWORDS:* inverse, Asian emissions, carbon monoxide

1.   Introduction

[2]   Understanding and predicting the atmospheric distribution of a chemical species requires information on the emissions of that species and of its precursors. The bottom-up approach to compiling emission inventories generally relies on emission factors for individual processes extrapolated in space and time using energy and environmental data. Top-down constraints from atmospheric

concentration measurements, interpreted with a chemical tracer model (CTM), can be used to improve the bottom-up estimates through an optimal estimation methodology (inverse model). Almost all global inverse modeling studies of emissions so far have used atmospheric concentrations measured from the NOAA/CMDL network of surface sites [e.g., *Hein et al.*, 1997; *Kaminski et al.*, 1999; *Bergamaschi et al.*, 2000; *Kasibhatla et al.*, 2002; *Pétron et al.*, 2002]. However, these sites are designed to monitor the remote atmosphere and are often not well situated to provide constraints on continental emissions of trace gases. We present here the first application of inverse modeling to
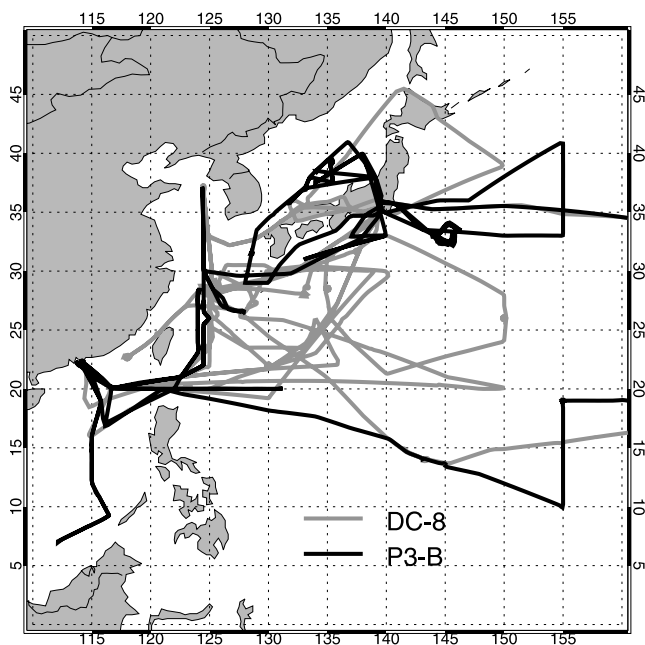
Figure 1. TRACE-P flight tracks for the DC-8 and P3-B aircraft. The inverse model is applied to the ensemble of data west of 150°E which includes 229 hours of CO measurements from the two aircraft, distributed over 28 flights from 27 February to 3 April 2001 [*Jacob et al.*, 2003]. See color version of this figure at back of this issue.

observations from an aircraft mission targeted at sampling continental outflow. As we will show, the high density of aircraft observations over a range of outflow pathways provides considerable information for inverse modeling and also allows us to quantify CTM transport errors for use in the inverse model. Our detailed specification of these errors represents a major advance over previous inverse model studies.

[3] We apply the inverse model approach to aircraft observations of carbon monoxide (CO) taken during the NASA Transport and Chemical Evolution over the Pacific (TRACE-P) mission in March–April 2001 [*Jacob et al.*, 2003]. The TRACE-P mission used two aircraft (DC-8 and P-3B), based in Hong Kong and Tokyo, to sample Asian chemical outflow along the Pacific rim (Figure 1). Carbon monoxide is a general product of incomplete combustion and has an atmospheric lifetime of a few months against oxidation by OH, its main sink. It provides the principal sink for OH, the main tropospheric oxidant, and plays therefore a critical role in controlling the oxidizing power of the atmosphere [*Logan et al.*, 1981]. It is also a useful atmospheric tracer for combustion sources. Previous inverse modeling studies of CO emissions [*Kasibhatla et al.*, 2002; *Pétron et al.*, 2002] have identified Asia as a region with large discrepancies between bottom-up inventories and atmospheric observations from the NOAA/CMDL network.

[4] Asian sources of CO during TRACE-P included anthropogenic emissions from fossil fuel and biofuel consumption, as well as seasonal biomass burning in Southeast Asia [*Streets et al.*, 2003; *Heald et al.*, 2003b].

The major meteorological processes driving outflow of anthropogenic Asian pollution during TRACE-P included lifting in warm conveyor belts (WCBs) ahead of south-eastward moving cold fronts and transport in the boundary layer behind these fronts [*Liu et al.*, 2003]. Outflow of biomass burning effluents from Southeast Asia took place both by deep convection and WCBs, the latter process leading to mixing with the anthropogenic outflow [*Ma et al.*, 2003; *Tang et al.*, 2003]. No evident plumes from Europe, North America, or Africa were sampled in TRACE-P, although these sources certainly contributed to the CO background [*Liu et al.*, 2003], as well as oxidation of CH_4 and biogenic nonmethane volatile organic compounds (NMVOCs).

[5] Our inversion analysis uses the TRACE-P aircraft observations, together with a priori information on Asian emissions from customized bottom-up inventories produced for the TRACE-P period [*Streets et al.*, 2003; *Heald et al.*, 2003a], to obtain optimized a posteriori estimates of CO emissions from different source regions in Asia. The maximum a posteriori inverse model approach has been used previously in three studies investigating the global emissions of CO [*Bergamaschi et al.*, 2000a; *Kasibhatla et al.*, 2002; *Pétron et al.*, 2002]. These studies all used the global measurements of CO from the NOAA/CMDL network [*Novelli et al.*, 1998] as top-down constraints, but they calculated global emissions from different years and lumped source types differently. *Bergamaschi et al.* [2000] calculated global emissions from separate sources as well as for total emissions in each hemisphere. They found that their bottom-up emission inventories were too low and attributed the cause either to anthropogenic emissions or to oxidation of biogenic terpenes. *Kasibhatla et al.* [2002] and *Pétron et al.* [2002] used a geographically disaggregated approach to identify emissions from specific regions and specific source types. Both these studies found that their a priori emissions from Asia were too low and reconciled this with the rapid industrialization of the region in recent years. Measurements at NOAA/CMDL stations have complex source signatures, because of their remote locations, limiting the level of useful disaggregation of CO sources to the continental scale. The TRACE-P aircraft data allows a more detailed disaggregation and a more focused assessment of CO emissions from Asia.

[6] In the next section we briefly describe the GEOS-CHEM CTM used here to simulate CO during TRACE-P and present a comparison between the modeled and measured concentrations of CO. Section 3 describes the inverse model and explores the potential of TRACE-P measurements to constrain emission estimates from particular geographical regions. Section 4 presents the inverse model analysis of the TRACE-P data and investigates the sensitivity of results to different assumptions. Section 5 places the results in the context of previous work. We conclude the paper in section 6.

2. GEOS-CHEM Model Simulation of CO During TRACE-P

2.1. Model Description

[7] The GEOS-CHEM global three-dimensional (3-D) model of tropospheric chemistry [*Bey et al.*, 2001a] is used

here to relate sources of CO to atmospheric concentrations and constitutes the forward model in the inverse analysis (section 3). A recent application of GEOS-CHEM to the global simulation of CO, including evaluation with the ensemble of NOAA/CMDL observations, is presented by B. N. Duncan et al. (Model study of the variability and trends in carbon monoxide (1988–1997): 1. Model formulation, evaluation, and sensitivity, submitted to *Journal of Geophysical Research*, 2003, hereinafter referred to as Duncan et al., submitted manuscript, 2003). The model version used here (v4.33, available at http://www-as.harvard.edu/chemistry/trop/geos/index.html) has a horizontal resolution of 2° latitude ×2.5° longitude and has 48 vertical levels ranging from the surface to the mesosphere, 20 of which are below 12 km. The model is driven by GEOS-3 assimilated meteorological data from the Goddard Earth Observing System (GEOS) of the NASA Data Assimilation Office. The 3-D meteorological data are updated every 6 hours; mixing depths and surface fields are updated every 3 hours.

[8] Gridded CO emission inventories for fossil fuel, biofuel, and biomass burning in East Asia during the TRACE-P period [*Streets et al.*, 2003; *Heald et al.*, 2003a] are used as a priori by the model. The *Streets et al.* [2003] inventory describes anthropogenic fossil fuel and biofuel emissions for the year 2000. Fossil fuel emissions are from residential coal and oil (both used for cooking and heating), transportation, and industry. Biofuel emissions (heating and cooking) are from wood, agricultural residues, and dung. We do not account for seasonal variability of any anthropogenic emissions because the TRACE-P sampling period is relatively short (March–April) and emissions are then near their annual mean value. *Streets et al.* [2003] provide detailed error estimates associated with their national emissions from Asia, representing important information for the inverse model analysis. Fossil and biofuel emissions for the rest of the world are taken from Duncan et al. (submitted manuscript, 2003) and *Yevich and Logan* [2003], respectively.

[9] We use daily biomass burning CO emissions for the TRACE-P period from *Heald et al.* [2003]. This inventory uses firecount data from the AVHRR satellite instrument [*Stroppiana et al.*, 2000] to constrain daily variability. It applies this variability to the biomass burning emission inventory of CO from *Duncan et al.* [2003], which includes interannual and seasonal variability derived from TOMS, ATSR, and AVHRR satellite observations. Global biomass burning emissions during TRACE-P were mainly from Southeast Asia and India and were approximately the same as the climatological average for February–April [*Heald et al.*, 2003]. Biomass burning emissions in eastern Asia during TRACE-P represent ≃75% of the annual total for that region and represent typically >50% of the global mean biomass burning emissions during February–April.

[10] In addition to direct emissions of CO there is a large chemical source from the oxidation of CH_4 and NMVOCs, which is treated here following the approach of Duncan et al. (submitted manuscript, 2003). Anthropogenic and biomass burning NMVOCs are in general coemitted with CO; following Duncan et al. (submitted manuscript, 2003), we model them here as direct sources of CO and correspondingly increase the primary emissions of CO by 20% (fossil
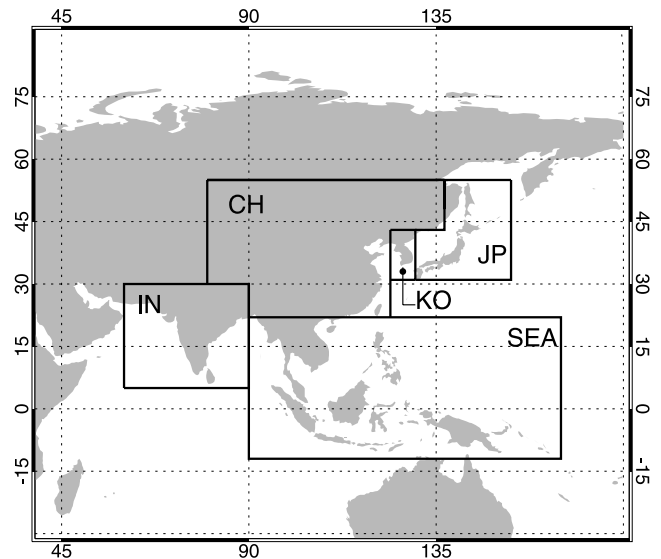
Figure 2. Source regions for tagged CO simulations. See Table 1 for emission estimates.

fuel) and 10% (biofuel and biomass burning). Additional sources of CO in the model include CH_4 (850 Tg CO/yr) and biogenic NMVOCs with contributions from isoprene (175 Tg CO/yr), methanol (85 Tg CO/yr), monoterpenes (70 Tg CO/yr), and acetone (25 Tg CO/yr). Further details on these sources can be found in the work of Duncan et al. (submitted manuscript, 2003). Oxidation of CH_4 by OH largely determined the chemical source of CO; emissions of shorter-lived biogenic NMVOCs are low during March–April and contribute only a few percent to the TRACE-P measurements.

[11] The main sink for CO is oxidation by OH. We use prescribed monthly mean OH concentration fields calculated from a full-chemistry simulation conducted with GEOS-CHEM v4.33. The corresponding lifetime of methylchloroform (CH_3CCl_3), a proxy for the global mean OH concentration, is 6.3 years; this is consistent with the best estimate of $5.99^{+0.95}_{-0.71}$ years by *Prinn et al.* [2001] from CH_3CCl_3 measurements. A detailed discussion of the factors affecting the CH_3CCl_3 lifetime in GEOS-CHEM is presented by *Martin et al.* [2003]. Although adjustment of CO sources in the inverse model analysis should modify OH, the effect is inconsequential for inverting Asian sources using the TRACE-P observations, which are only a few days downwind of the sources. Correction to OH is effectively taken into account in the inversion through the adjustment of the CO source from ''rest of the world'' (section 4). The assumption of fixed OH linearises the inverse problem [*Pétron et al.*, 2002]. In the forward model we ''tag'' CO produced by different sources from different geographic regions (Figure 2, Table 1). The Jacobian matrix **K** for the inversion (section 3.1), relating individual annual mean sources of CO to the resulting atmospheric concentrations, can then be readily calculated by dividing a particular tagged member by its respective annual emission.

[12] A number of previous GEOS-CHEM model studies have evaluated the simulation of CO with surface and aircraft observations in different regions of the world [*Bey et al.*, 2001a, 2001b; *Fiore et al.*, 2002; *Li et al.*, 2002; *Martin*

Table 1. Annual A Priori Sources of CO (Tg CO yr^{-1}) for the Inverse Model Analysis

Region	Biofuels[a] (BF)	Fossil Fuel[a] (FF)	Biomass Burning[a] (BB)	Methane and Biogenic NMVOCs
China (CH)	45±35	64 ± 50	19 ± 9	
Korea (KR)	4 ± 2	5 ± 2	0.3 ± 0.1	
Japan (JP)	2 ± 0.4	7 ± 1	0.8 ± 0.4	
India (IN)	38 ± 38	16 ± 16	39 ± 19	
Southeast Asia (SEA)	26 ± 26	17 ± 17	82 ± 41	
Rest of World (RW)	70 ± 35	273 ± 96	340 ± 170	
TOTAL	185 ± 68	382 ± 110	481 ± 176	1205 ± 301

[a]Sources from BF, BB, and FF include the secondary source of CO from the oxidation of NMVOCs coemitted with CO.

et al., 2003; *Kasibhatla et al.*, 2002; Duncan et al., submitted manuscript, 2003]. These studies used earlier versions of GEOS-CHEM, with different CO sources and OH concentrations, so that results are not strictly comparable. The global underestimate of CO reported in the original version of GEOS-CHEM [*Bey et al.*, 2001a] has since been corrected by better accounting of NMVOC precursors and of various factors acting to reduce OH [*Martin et al.*, 2003; Duncan et al., submitted manuscript, 2003]. The most recent global evaluation (Duncan et al., submitted manuscript, 2003) indicates no bias in the simulation of the CO background, and this appears to hold also for v4.33 used here [*Heald et al.*, 2003]. However, both (Duncan et al., submitted manuscript, 2003) and *Heald et al.* [2003] used an anthropogenic Chinese source of CO that is 20% higher than the *Streets et al.* [2003] inventory used here.

[13] The timing of TRACE-P (February–April) was chosen to coincide with the strongest outflow from Asia to the Pacific, driven by frequent wave cyclones and associated cold fronts and warm conveyor belts [*Yienger et al.*, 2000; *Bey et al.*, 2001b], and to encompass the biomass burning season in Southeast Asia which peaks typically in March [*Duncan et al.*, 2003]. Anthropogenic emissions are largely aseasonal. TRACE-P was conducted early in the growing season so the source of CO from biogenic emissions represents only a few percent of the total measured outflow of CO from Asia.

2.2. TRACE-P Measurements of CO

[14] Diode laser spectroscopic measurements of CO were taken during TRACE-P using the Differential Absorption CO Measurement (DACOM instrument) [*Sachse et al.*, 1987]. CO was measured at a frequency of 1 Hz with an estimated 1-s precision of 1%. We use here the 1-min average data and further average it over the GEOS-CHEM $2 \times 2.5°$ grid along the flight tracks; for the purpose of our analyses these subsequent values are what we use as observations. Accuracy of the 1-min averaged data is ≃2% and is dominated by the accuracy of the NOAA/ CMDL calibration standards (Paul Novelli, NOAA/CMDL, personal communication, 2003). Altitude ranges for the DC-8 and P3-B aircraft flight tracks are 0–12 km and 0–10 km, respectively.

[15] The GEOS-CHEM global 3-D simulations of CO and tagged CO tracers were initialised in January 2000 and conducted for 16 months (through April 2001). The 14-month simulation before the start of TRACE-P effectively removes the influence from initial conditions. We sample the model fields along TRACE-P flight tracks and compare with the observations averaged over the $2 \times 2.5°$ model grid. We remove the influence of stratospheric air using the criterion $O_3 > 100$ ppb; we verified that this does not remove any pollution plumes (O_3 was occasionally above 100 ppb in Chinese urban plumes but not when averaged over the $2 \times 2.5°$ grid). We also ignore data east of 150°E, which are mainly from transit flights (Figure 1). The data used for the inversion include all flights between 27 February and 3 April 2001.

2.3. Evaluation of Model With A Priori Sources

[16] Before proceeding with the inversion we first examine the ability of the a priori sources, as described in section 2.1, to simulate the TRACE-P measurements of CO (section 2.2). A general statistical comparison of model results with observations is shown in Figure 3. The model is on average 23 ppb too low; this discrepancy is driven by the high tail of the distribution (CO > 200 ppb), representing strong boundary layer outflow from Asia. The frequency distribution of differences at model and observations shows an approximate Gaussian distribution with a 13 ppb negative bias in the median. Major pollution plumes in the observations (CO > 500 ppb) are not well captured by the model.

[17] A more detailed evaluation of the model with observations is shown in Figure 4 by the modeled and observed latitudinal gradients at different altitudes from 0 to 12 km. The model has a negative bias in the boundary layer which increases with latitude, reaching 80 ppb (30% of the mean total CO) between 30 and 40°N. We attribute this negative bias to an underestimate of Chinese anthropogenic emissions, as discussed below. Above the boundary layer the negative model bias is less, and largely disappears south of 30°N or above 6 km. The concentration of CO in the free troposphere is relatively more sensitive to biomass burning and to sources outside of Asia [*Liu et al.*, 2003].

3. Inverse Model

3.1. Description

[18] Measured concentrations of CO (assembled in a measurement vector **y**), are related to the sources of CO (assembled in a state vector **x**) by the following relation [*Rodgers*, 1976]:

$$\mathbf{y} = \mathbf{Kx} + \boldsymbol{\epsilon}. \qquad (1)$$

The state vector **x** as defined here comprises annual source estimates from different geopolitical regions and from different CO source types; its composition will be discussed
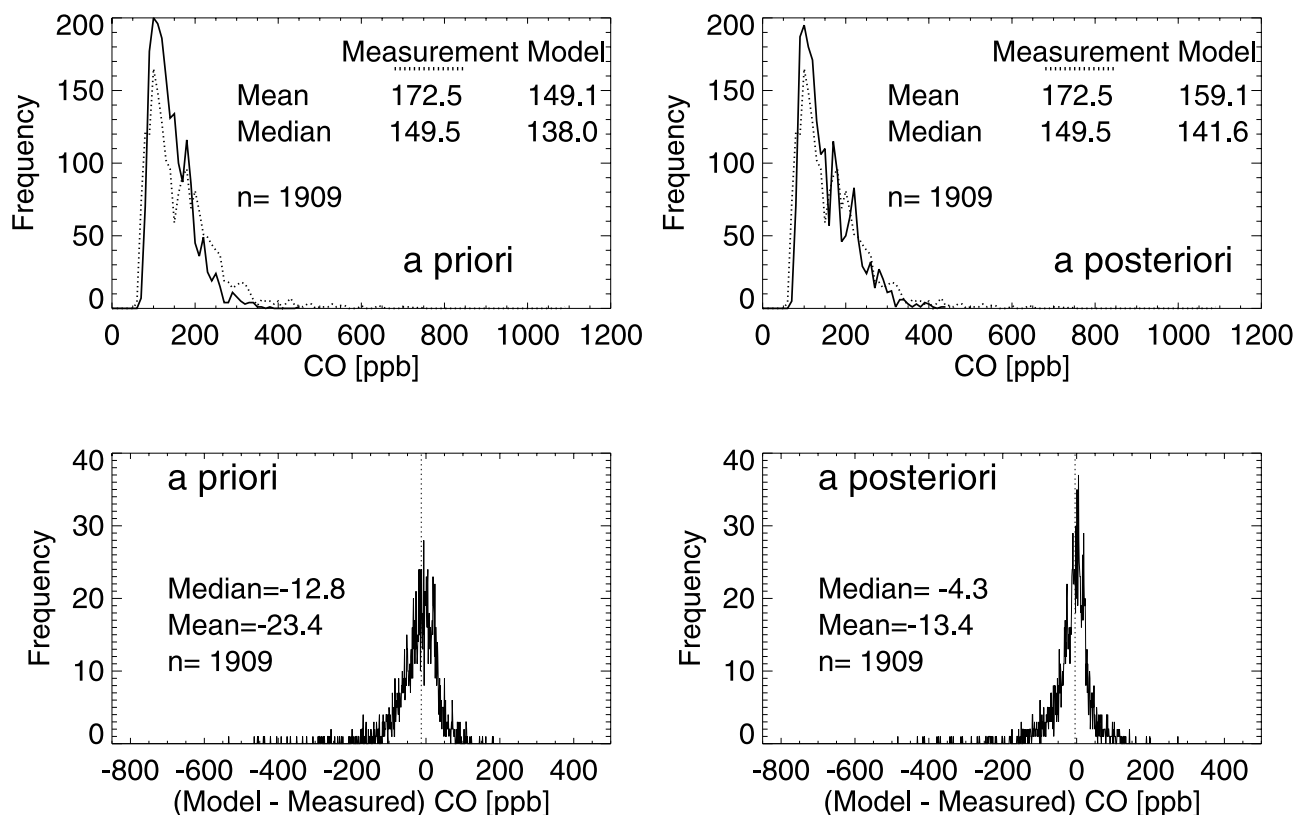
Figure 3. Statistical comparison of simulated and observed CO from TRACE-P, for the model with a priori sources (left panels) and a posteriori sources (right panels). The observations have been averaged over the $2 \times 2.5°$ model grid. Data influenced by the stratosphere ($O_3 > 100$ ppb) or away from the western Pacific rim (longitudes $>150°E$) are excluded from the comparison. Top: frequency distributions of simulated (solid) and observed (dotted) CO. Bottom: frequency distribution of the difference between simulated and observed CO.

in section 3.3. Although the TRACE-P observations do not actually constrain the annual mean source, but rather the source integrated over some time horizon determined by the transport and lifetime of CO, it is clearer to express $\mathbf{x}$ in terms of annual sources and assume that the model seasonal variation for these sources is correct. The measurement vector $\mathbf{y}$ comprises the TRACE-P CO mixing ratio data averaged along the flight tracks over the model grid. The Jacobian matrix $\mathbf{K}$, as described in section 2.1, describes the forward model and does not depend on the state vector under our linear assumption. The error vector $\boldsymbol{\epsilon}$ includes contributions from measurement accuracy, subgrid variability of observations (representation error), and errors in model parameters (transport, chemistry, subregional emission patterns). The ensemble characteristics of these errors are described by the observation error covariance $\mathbf{S}_\Sigma$, representing a sum of the covariance matrices from individual sources of error.

[19] An inverse model describes the mathematical mapping from the measurement vector space to the state vector space. Here the inverse model describes the best estimate of sources of CO that is consistent with both the aircraft observations of CO concentration during TRACE-P and the a priori sources of CO, given their respective uncertainties. The fundamental idea of an optimal estimation inverse method is to minimize a cost function $\mathbf{J}(\mathbf{x})$ (that is, to solve

$\nabla_{\mathbf{x}}\mathbf{J}(\mathbf{x}) = 0$). We use a standard least-squares formulation for $\mathbf{J}(\mathbf{x})$:

$$\mathbf{J}(\mathbf{x}) = (\mathbf{y} - \mathbf{K}\mathbf{x})^{\mathrm{T}}\mathbf{S}_\Sigma^{-1}(\mathbf{y} - \mathbf{K}\mathbf{x}) + (\mathbf{x} - \mathbf{x}_a)^{\mathrm{T}}\mathbf{S}_a^{-1}(\mathbf{x} - \mathbf{x}_a), \quad (2)$$

where $\mathbf{x}_a$ is the a priori value of the state vector (comprised of the a priori sources), $\mathbf{S}_a$ is the estimated error covariance matrix for $\mathbf{x}_a$, and all other variables are as defined previously. Solution to $\nabla_{\mathbf{x}}\mathbf{J}(\mathbf{x}) = 0$ yields [*Rodgers*, 2000]
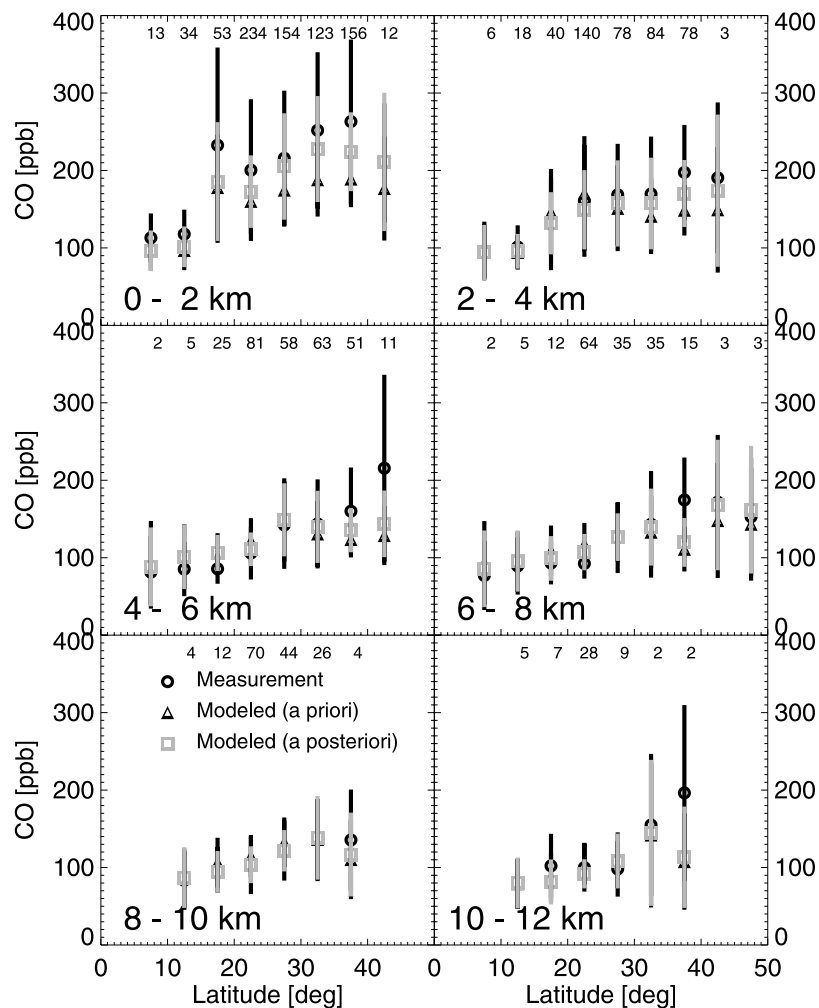
$$\hat{\mathbf{x}} = \mathbf{x}_a + \left(\mathbf{K}^{\mathrm{T}}\mathbf{S}_\Sigma^{-1}\mathbf{K} + \mathbf{S}_a^{-1}\right)^{-1}\mathbf{K}^{\mathrm{T}}\mathbf{S}_\Sigma^{-1}(\mathbf{y} - \mathbf{K}\mathbf{x}_a) \quad (3)$$

$$\hat{\mathbf{S}} = \left(\mathbf{K}^{\mathrm{T}}\mathbf{S}_\Sigma^{-1}\mathbf{K} + \mathbf{S}_a^{-1}\right)^{-1}, \quad (4)$$

where $\hat{\mathbf{x}}$ is the optimized a posteriori state vector and $\hat{\mathbf{S}}$ is the a posteriori error covariance matrix, describing the error on $\hat{\mathbf{x}}$. The value of the cost function before and after all the observations have been ingested provides a useful indication of the quality of the inversion. In a successful inversion, $\mathbf{J}(\mathbf{x})$ should be of the same order as the number of observations, provided that $\mathbf{S}_\Sigma^{-1}$ and $\mathbf{S}_a$ are properly specified.

3.2. Error Specification

[20] The Asian emission inventory of *Streets et al.* [2003], used here to define the a priori state vector $\mathbf{x}_a$,

Figure 4. Latitudinal gradients of measured and modeled CO concentrations over the TRACE-P domain on a 2 × 2.5° grid. Observations (circles) are averaged over the altitude range shown in the figure, and over 5° latitude bins. Vertical bars denote 1-σ values about the mean. The model is sampled along the TRACE-P flight tracks for the flight days, and values are averaged across the same latitude and altitude ranges as the observations. Model values are shown for the simulations with a priori (triangles) and a posteriori (squares) sources. Data influenced by the stratosphere (O₃ > 100 ppb) or away from the western Pacific rim (longitudes >150°E) have been excluded from the comparison. Numbers inset at the top of each panel refer to the number of observations used to compute the mean statistics. See color version of this figure at back of this issue.

includes uncertainty estimates for individual countries and processes derived by propagation of errors in the bottom-up approach. These uncertainties are listed in Table 1. We aggregate emissions from North America and Europe (assigned an uncertainty of 30%) and other countries outside of Asia (assigned an uncertainty of 50%) in to the "rest of the world" source (section 3.3); TRACE-P was not designed to provide information on these regions so detailed specification of errors is not essential. We assign the source from biomass burning an uncertainty of 50%. The chemical source from oxidation of CH_4 and biogenic NMVOCs is defined largely by CH_4, and we assign it an uncertainty of 25% based on constraints on global OH from observations of CH_3CCl_3 [*Prather and Enhalt*, 2001]. The sensitivity of the a posteriori solution to the assumed emission uncertainties will be assessed in section 4.

[21] The total observation error S_Σ includes contributions from measurement accuracy, representation error, and errors in the forward model. Estimating errors due to the model is nontrivial. We do so here by computing the statistics of the relative difference between the aircraft observations and the colocated model mixing ratios, $(Kx_a - y)/y$, as a function of altitude and for two latitude ranges (Figure 5). We assume that the mean model bias, as diagnosed by the mean relative difference, is due to errors in the a priori sources and that the variance about this mean value represents errors due to the model. This assumption is unlikely to be strictly true because there is a contribution from emission errors in the variance and a contribution from model physics in the bias, but as we shall show below our approach appears to be reasonable. An intercomparison of CTM simulations of CO during the TRACE-P period [*Kiley et al.*, 2003] showed no evident bias

A priori
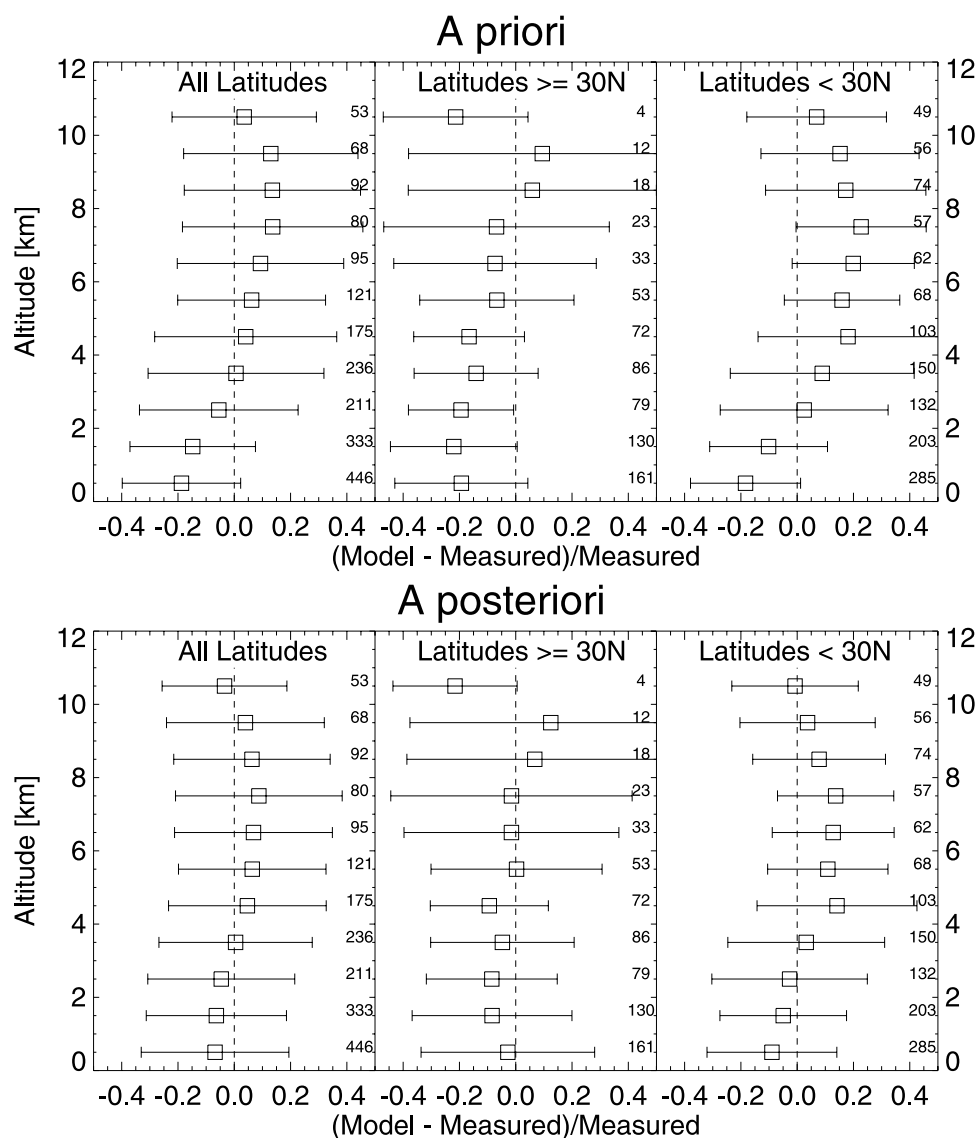
A posteriori

Figure 5. Relative GEOS-CHEM model errors in the simulation of CO during TRACE-P, as a function of altitude for the model with a priori sources of CO (top) and with a posteriori sources (bottom). Squares denote the mean bias and horizontal lines denote 1-σ values about the mean. Numbers inset of each panel refer to the number of observations used to compute statistics at each altitude.

in GEOS-CHEM transport. By subtracting the mean bias for each altitude and latitude range in Figure 5 we are left with the residual relative error (RRE). Then for each individual observation y_i at a particular latitude (north or south of 30°N) and altitude we calculate an absolute model error as RRE × y_i. We assume no error covariance between observations. CO observations are 1-min average measurements that have been averaged spatially over our 2 × 2.5° model grid and averaged temporally over complete flights. Correlation of the errors between observations over these spatial and temporal scales are small and do not affect the results shown here significantly. Typical values for the RRE are between 0.2 and 0.3, as can be seen from Figure 5. The RREs calculated from the simulation with a priori sources show higher values in the free troposphere, but this difference is substantially reduced in the simulation with a posteriori sources, discussed below.

[22] Values of the mean bias as shown in Figure 5 are consistent with those reported in Figure 3. The TRACE-P domain (Figure 1) can be split into two distinct regions, characterized by differences in air masses sampled [*Blake et al.*, 2003]. North of 30°N, air masses were heavily influenced by fossil fuel and biofuel emissions from China, Korea and Japan; below 2 km there was essentially no influence from biomass burning [*Liu et al.*, 2003]. South 30°N and in particular the free troposphere air masses were more influenced by biomass burning. Mean bias statistics for both north and south of 30°N show an underestimate of emissions in the boundary layer. In the free troposphere, there is still a small underestimate above 30°N but an overestimate at lower latitudes. These mean bias statistics suggest that a priori anthropogenic emissions are too low, while biomass burning emissions are too high.

[23] Our method of quantifying model transport error is a major advance over previous inverse model studies which have estimated the total observation error by calculating the standard deviation of the discrepancy between model and

measured monthly mean values in the surface data used for the inversions [e.g., *Bousquet et al.*, 1999; *Kasibhatla et al.* 2002]. Our method can be used iteratively to improve the estimate for model errors. To illustrate this we recalculated values of RRE using the a posteriori CO sources (to be presented in section 4). We find that the a posteriori sources, although they reduce greatly the bias between simulated and observed concentrations, yield values of RRE that are comparable with those calculated using a priori emissions. This supports our assumption that the mean bias is largely due to errors in the emissions and the variability is due to errors in the transport.

[24] Additional errors contributing to S_Σ include measurement accuracy ($\simeq 2\%$ of the concentration) and representation error, describing the mismatch between the model and observations due to subgrid scale variability. We quantify the representation error by examining statistics of the subgrid variability in the observations over the $2 \times 2.5°$ GEOS-CHEM model grid. We compute this error for each sampled model grid cell and find that it is typically 5–10% of the observed concentration. We thus find in our error analysis that the model error represents typically 73% (mean = 38 ppb) of the total observation error budget and is therefore the most important to quantify, representation error accounts for approximately 25% (mean = 14 ppb), and instrument accuracy accounts for the remaining 2% (mean = 2 ppb).

3.3. Selection of State Vector

[25] The ability of the observing system to determine different elements of the state vector, taking into account the assigned measurement and a priori state uncertainties, can be tested by inspecting the matrix of averaging kernels $\mathbf{A} = \mathbf{I} - \hat{\mathbf{S}}\mathbf{S}_a^{-1}$, where $\mathbf{I}$ is the identity matrix, and $\hat{\mathbf{S}}$ is computed from equation (4) [*Kasibhatla et al.*, 2002]. Averaging kernels peaked at their own state vector element denote a well constrained source. Starting from the ensemble of source regions and processes in Table 1, we used averaging kernels (not shown) to determine which sources or aggregation of sources could be constrained independently with the TRACE-P data. We find that fossil fuel and biofuel emissions within a given country are too colocated to be retrieved independently [*Kasibhatla et al.*, 2002], and such is the case also for biomass burning except for China. Indian airmasses sampled during TRACE-P are mostly from biomass burning and contribute typically less than a few percent to the total CO measured during TRACE-P. We aggregate these emissions with rest of the world (RW). We must also aggregate emissions from Japan and Korea, as TRACE-P does not provide independent information on the two (Japanese outflow sampled in TRACE-P had generally passed previously over Korea [*Palmer et al.*, 2003]). The source of CO from the oxidation of CH_4 and biogenic NMVOCs is aggregated into the RW source.

[26] We thus define a five-component state vector (CHBFFF, KRJP, SEA, CHBB, RW) for which the averaging kernels are shown in Figure 6. Even with this aggregated state vector there is poor definition of the combined Korea and Japan source, reflecting the relatively small uncertainties assigned by *Streets et al.* [2003] for a priori emissions from these countries (Table 1); increasing the uncertainty on these a priori emissions improves their

resolution. We also find that the Chinese biomass burning source is slightly correlated with the non-Asian source of CO (rest of the world); both of these sources affect mostly the free troposphere in the TRACE-P observations.

4. Results

[27] We apply the optimal inverse model described in the previous section to the TRACE-P data. We use a χ^2 quality control test to remove outliers (4% of the data), leaving 1825 observations. Results shown in Table 2 indicate a 54% increase in a posteriori anthropogenic emissions from China relative to the a priori, a 74% decrease in emissions from Southeast Asia (mostly from biomass burning, see Table 1), and smaller relative changes in other sources. The increase in Chinese anthropogenic emissions is driven by the model underestimate in the boundary layer (Figure 4 and Figure 5), while the decrease in biomass burning derives from the model overestimate in the free troposphere (Figure 4 and Figure 5). There is a 7% increase in the source from the rest of the world (135 Tg CO yr^{-1}) which represents effectively an adjustment in the background CO.

[28] We can test the utility of the inverse model by using the a posteriori emissions with the tagged tracers in the forward model to simulate the TRACE-P observations. Comparison with observations is improved (Figure 3). The median value of the difference between model and observed CO decreases from −13 ppb to −4 ppb, while the mean bias is reduced by 30%. The frequency distribution of the differences is more peaked around zero. Figure 4 shows that in general the a posteriori emissions simulate the observed latitudinal variability of CO better than the a priori emissions, significantly reducing the large discrepancies in the boundary layer and elsewhere. The value of the cost function (equation (2)) decreases from 2120 with a priori sources to 1604 with a posteriori sources. The latter value is slightly less than the number of observations ($n = 1825$), indicating a successful inversion.

[29] The inverse model approach is sensitive to uncertainties assumed for the observations (S_Σ) and the a priori emissions (S_a) (equation (4)). Model error largely defines S_Σ (section 3). We find that doubling and halving S_a or the model error does not affect significantly the results of the inversion, suggesting that our best estimate of a posteriori sources is robust (Figure 7). Doubling S_a has the same effect on the inversion as halving model error, and vice versa. Doubling the uncertainty of a priori emissions from KRJP improves the resolution of that source (section 3.3) which then increases by +68% (as compared with +26% in the standard inversion). Fixing the RW source to its a priori value and inverting for the other sources, equivalent to assuming perfect knowledge of background CO, alters many of the a posteriori sources (not shown) but does not change the general tendency of our best estimate: anthropogenic emissions increase (CHBFFF, KRJP) and biomass burning emissions decrease (CHBB, SEA).

5. Comparison With Previous Work

[30] *Kiley et al.* [2003] presented an intercomparison of TRACE-P CO simulations from seven different CTMs using the *Streets et al.* [2003] emission inventory for Asia.
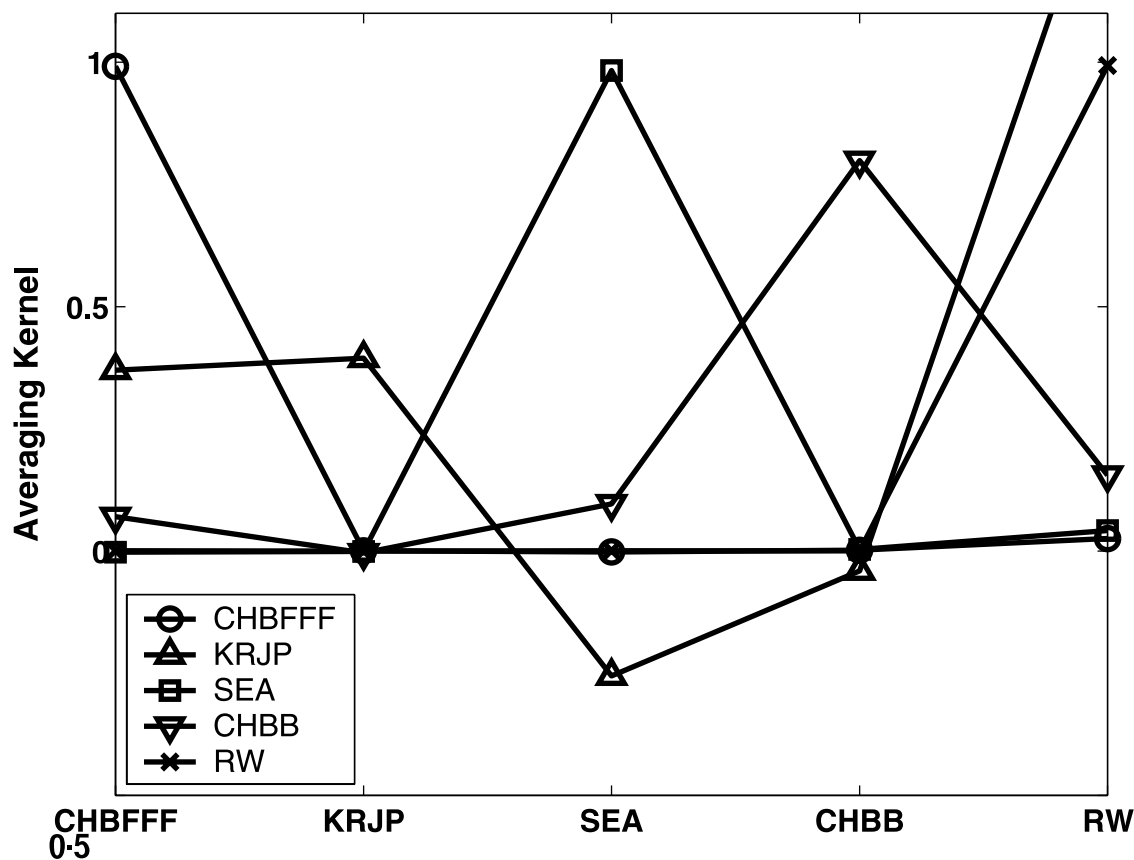
Figure 6. Individual rows of the averaging kernel matrix **A** for the inversion of CO sources with the TRACE-P observing system. Different colors distinguish rows of **A**, listed in the legend, with the corresponding columns indicated on the x-axis. Lines connect the symbols for clarity and do not have any physical significance. The five-element state vector includes sources from Chinese fuel consumption (CHBFFF), total emissions from Korea and Japan (KRJP), total emissions from Southeast Asia (SEA), Chinese biomass burning (CHBB), and the rest of the world (RW) including the chemical source of CO from the oxidation of CH_4 and biogenic NMVOCs. See color version of this figure at back of this issue.

All models found an underestimate of CO in the boundary layer, consistent with the results presented here and which we attribute to a 54% underestimate of anthropogenic Chinese emissions (a posteriori emission value = 168 Tg CO/yr). *Carmichael et al.* [2003] also investigated this underestimate of Chinese CO with a regional CTM and attributed it to an underestimate in emissions from the domestic combustion sector, in particular from residential coal burning. They tentatively suggest that a factor of 3−5 increase in the *Streets et al.* [2003] inventory for that sector would be required to reconcile model results with the observed concentrations. Such an increase would correspond to Chinese anthropogenic emissions of 169−228 Tg CO/yr, a value not inconsistent with the value presented here.

[31] Our a posteriori biomass burning emissions for Southeast Asia and China are considerably lower than the a priori values. This result is qualitatively consistent with CO column data from the MOPITT satellite instrument during TRACE-P, which imply much lower biomass burning emissions in Southeast Asia and Northeast India than used here as a priori [*Heald et al.*, 2003b]. Correlations of CO with HCN in the TRACE-P data, with HCN taken as a tracer of biomass burning, do not imply an overestimate of biomass burning CO emissions [*Li et al.*, 2003]. However, anthropogenic Chinese sources of HCN may complicate this interpretation [*Singh et al.*, 2003].

[32] Specific investigation of biomass burning influences in the TRACE-P data was conducted by *Carmichael et al.* [2003] and *Tang et al.* [2003] using their regional CTM with Asian biomass burning emissions (67 Tg CO/yr) that are a factor of two smaller than our a priori values. *Carmichael et al.* [2003] used back-trajectories to construct the spatial distributions of emissions corresponding to the observed versus simulated TRACE-P CO concentrations. They found

Table 2. A Priori and A Posteriori Annual Source Magnitudes of CO (Tg CO yr^{-1})

State Vector Element	A Priori	A Posteriori	Δ%
CHBFFF	109 ± 61	168 ± 5	+54
KRJP	19 ± 3	24 ± 2	+26
SEA	125 ± 51	33 ± 7	−74
CHBB	19 ± 9	12 ± 4	−37
RW	1981 ± 380	2117 ± 31	+7
TOTAL	2253 ± 388	2353 ± 32	+4
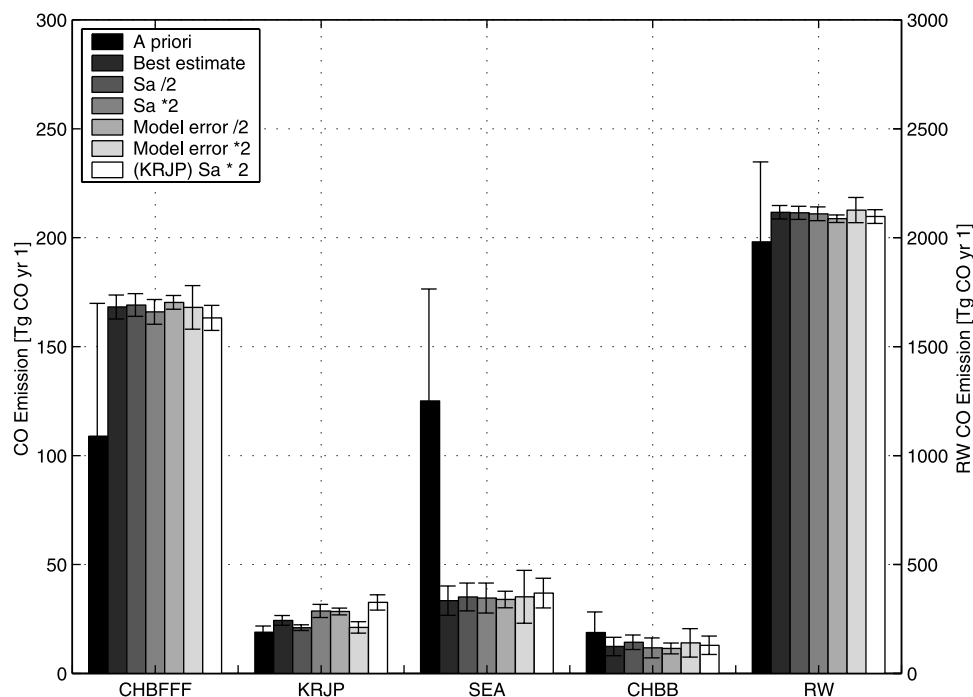
Figure 7. Sensitivity of the calculated a posteriori sources to the error estimates in the inverse model. Vertical bars denote 1-σ value from Ŝ. "Best estimate" shows the a posteriori source from the standard inversion (Table 2). A posteriori sources derived from inversions with modified errors on the a priori source (S_a) or on the model error are also shown. Elements in the abscissa are as in Figure 6. See color version of this figure at back of this issue.

large differences between the two over biomass burning regions of Southeast Asia and Northeast India, implying errors either in model sources or model transport.

[33] *Kasibhatla et al.* [2002] and *Pétron et al.* [2002] previously used CO observations from the NOAA/CMDL network [*Novelli et al.*, 1998] to determine regional sources of CO. Both found that their a priori Asian emissions, taken from the EDGAR inventory version 2.0 [*Olivier et al.*, 1996], were too low. *Kasibhatla et al.* [2002] showed that a 50% increase in Asian fuel consumption (to 350–380 Tg CO/yr) and a 100% increase in Asian biomass burning emissions (to 110–130 Tg CO/yr) were required to reconcile the NOAA/CMDL concentration data from 1994; *Pétron et al.* [2002], using average NOAA/CMDL data for 1990–1996, required a factor of two increase in Asian anthropogenic emissions (to 548 Tg CO/yr) and a 25% increase in emissions from biomass burning (to 90 Tg CO/yr). Our a posteriori anthropogenic source of CO from Asia (186–198 Tg CO/yr, CHBFFF + KRJP, Table 2) is less than that derived in these two studies, and our a posteriori biomass burning source of CO (34–56 Tg CO/yr) is much lower. Values for the source of CO from the rest of the world, including the global source from chemical oxidation, are reported by *Kasibhatla et al.* [2002] (2240 Tg CO yr^{-1}) and *Pétron et al.* [2002] (2340 Tg CO yr^{-1}) but they are not strictly comparable with the value we report (2117 Tg CO yr^{-1}) because the TRACE-P data are largely insensitive to sources in regions outside of Asia.

[34] Some of our differences with *Kasibhatla et al.* [2002] and *Pétron et al.* [2002] can be attributed to the type of observations used. They used NOAA/CMDL sur-

face observations which are not intended to sample continental air masses. By the time such air masses are sampled at these remote surface sites their source signatures are highly mixed and consequently are difficult to separate. Simulating accurately these remote station data will be hampered by an accumulation of errors in model transport which weakens the sensitivity to continental sources. This can be compensated to some degree by the long-term nature of the NOAA/CMDL records.

6. Conclusions

[35] We used aircraft observations of Asian outflow from the TRACE-P mission (March–April 2001) to improve estimates of CO emissions from Asia using an optimal estimation inverse method. This is the first time than an inverse model has been applied to infer emissions from a large geopolitical source region using aircraft observations. We showed that the high density of coverage from an aircraft mission allows quantification of model transport error, a notorious difficulty in inverse modeling.

[36] We used the GEOS-CHEM global 3-D model of tropospheric chemistry, driven by customized a priori bottom-up emission inventories for Asia [*Streets et al.*, 2003; *Heald et al.*, 2003a] as a forward model to simulate the aircraft observations. The *Streets et al.* [2003] inventory includes a detailed error budget which provides important information for the inverse model calculation. Errors associated with the observations in the context of the inverse model include errors in model transport and other model parameters, representation error due to the inability of the

model to simulate observed subgrid scale structure, and instrument accuracy. We describe a new method of quantifying model errors by using the mean difference statistics between the simulated and observed CO concentrations, exploiting the high density of observations available from the aircraft mission. Mean bias between the model (with a priori emissions) and the observations is assumed to reflect errors in emissions, while the relative variance about this mean bias is assumed to reflect errors in transport. The model transport errors derived in that manner are in the range 20–30%. The representation error, estimated from the observed subgrid variability in the aircraft CO data, is typically 5–10%. Instrument accuracy ($\simeq$2%) is negligibly small relative to the other sources of error.

[37] Our inverse model analysis implies a 54% increase in Chinese anthropogenic emissions of CO (to 168 Tg CO yr^{-1}) relative to the a priori. A posteriori anthropogenic emissions from other Asian countries are not so different from their a priori values. Our best estimate of Asian anthropogenic emissions is lower than previous model studies that used sparse surface observations of CO as constraints [*Kasibhatla et al.*, 2002; *Pétron et al.*, 2002]. We find that a priori emissions of CO from biomass burning in Southeast Asia are too high, consistent with MOPITT observations during TRACE-P [*Heald et al.*, 2003b].

[38] Our future work will exploit the correlations of CO with other species to improve the top-down constraints for the inversion of the TRACE-P observations. For example, including CH_3CN in the inverse model analysis should provide valuable constraints on emissions of CO from biomass burning [*Li et al.*, 2002; *Singh et al.*, 2003]. Including CO_2 should help to disaggregate emissions from Korea and Japan whose CO_2/CO emission ratios are very different (P. Suntharalingam et al., Constraints of Asian carbon fluxes using CO_2/CO correlation from TRACE-P, submitted to Journal of Geophysical Research, 2003).

References

Bergamaschi, P., R. Hein, M. Heimann, and P. J. Crutzen, Inverse modeling of the global CO cycle: 1. Inversion of CO mixing ratios, *J. Geophys. Res.*, 105, 1909–1927, 2000.

Bey, I., et al., Global modeling of tropospheric chemistry with assimilated meteorology: Model description and evaluation, *J. Geophys. Res.*, 106, 23,073–23,096, 2001a.

Bey, I., D. J. Jacob, J. A. Logan, and R. M. Yantosca, Asian chemical outflow to the Pacific: Origins, pathways and budgets, *J. Geophys. Res.*, 106, 23,097–23,114, 2001b.

Blake, N. C., et al., NMHCs and halocarbons in Asian continental ouflow during TRACE-P: Comparison to PEM-West B, *J. Geophys. Res.*, 108(D20), 8806, doi:10.1029/2002JD003367, in press, 2003.

Bousquet, P., P. Ciais, P. Peylin, M. Ramonet, and P. Monfray, Inverse modeling of annual atmospheric CO_2 sources and sink: 1. Method and control inversion, *J. Geophys. Res.*, 104, 26,161–26,178, 1999.

Carmichael, G. R., et al., Regional-scale chemical transport modeling in support of intensive field experiments: Overview and analysis of the TRACE-P observations, *J. Geophys. Res.*, 108(D21), 8823, doi:10.1029/2003JD003117, in press, 2003.

Duncan, B. N., R. V. Martin, A. C. Staudt, R. Yevich, and J. A. Logan, Interannual and seasonal variability of biomass burning emissions con-

strained by satellite observations, *J. Geophys. Res.*, 108(D2), 4100, doi:10.1029/2002JD002378, 2003.

Fiore, A. M., D. J. Jacob, I. Bey, R. M. Yantosca, B. D. Field, and J. Wilkinson, Background ozone over the United States in summer: Origin and contribution to pollution episodes, *J. Geophys. Res.*, 107(D15), 4275, doi:10.1029/2001JD000982, 2002.

Heald, C. L., D. J. Jacob, P. I. Palmer, M. J. Evans, G. W. Sachse, H. B. Singh, and D. R. Blake, Biomass burning emission inventory with daily resolution: Application to aircraft observations of Asian outflow, *J. Geophys. Res.*, 108(D21), 8811, doi:10.1029/2002JD003082, in press, 2003a.

Heald, C. L., et al., Asian outflow and transpacific transport of carbon monoxide and ozone pollution: An integrated satellite, aircraft, and model perspective, *J. Geophys. Res.*, 108, doi:10.1029/2003JD003507, in press, 2003b.

Hein, R., P. J. Crutzen, and M. Heimann, An inverse modeling approach to investigate the global atmospheric methane cycle, *Global Biogeochem. Cycles*, 11, 43–76, 1997.

Jacob, D. J., J. Crawford, M. M. Kleb, V. S. Connors, R. J. Bendura, J. L. Raper, G. W. Sachse, J. Gille, L. Emmons, and J. C. Heald, Tranport and Chemical Evolution over the Pacific (TRACE-P) mission: Design, execution, and first results, *J. Geophys. Res.*, 108(D20), 8781, doi:10.1029/2002JD003276, in press, 2003.

Kaminski, T., M. Heimann, and R. Giering, A coarse grid three-dimensional global inverse model of the atmospheric transport: 2. Inversion of the transport of CO_2 in the 1980s, *J. Geophys. Res.*, 105, 18,555–18,581, 1999.

Kasibhatla, P., A. Arellano, J. A. Logan, P. I. Palmer, and P. Novelli, Top-down estimate of a large source of atmospheric carbon monoxide associated with fuel combustion in Asia, *Geophys. Res. Lett.*, 29(19), 1900, doi:10.1029/2002GL015581, 2002.

Kiley, C. M., et al., An intercomparison and evaluation of aircraft-derived and simulated CO from seven chemical transport models during the TRACE-P experiment, *J. Geophys. Res.*, 108(D21), 8819, doi:10.1029/2002JD003089, in press, 2003.

Li, Q., et al., Transatlantic transport of pollution and its effects on surface ozone in Europe and North America, *J. Geophys. Res.*, 1087(D13), 4166, doi:10.1029/2001JD001422, 2002.

Li, Q., D. J. Jacob, R. M. Yantosca, C. L. Heald, H. B. Singh, M. Koike, Y. Zhao, G. W. Sachse, and D. G. Streets, A global three-dimensional model analysis of the atmospheric budgets of HCN and CH_3CN: Constraint from aircraft and ground measurements, *J. Geophys. Res.*, 108(D21), 8827, doi:10.1029/2002JD003075, in press, 2003.

Liu, H., D. J. Jacob, I. Bey, R. M. Yantosca, B. N. Duncan, and G. W. Sachse, Transport pathways for Asian combustion outflow over the Pacific: Interannual and seasonal variations, *J. Geophys. Res.*, 108(D20), 8786, doi:10.1029/2002JD3102, in press, 2003.

Logan, J. A., M. J. Prather, S. C. Wofsy, and M. B. McElroy, Tropospheric chemistry: A global perspective, *J. Geophys. Res.*, 86, 7210–7254, 1981.

Ma, Y., et al., The characteristics and influence of biomass burning aerosols on fine particle ionic composition measured in Asian outflow during TRACE-P, *J. Geophys. Res.*, 108(D21), 8816, doi:10.1029/2002JD003128, in press, 2003.

Martin, R. V., D. J. Jacob, R. M. Yantosca, M. Chin, and P. Ginoux, Global and regional decreases in tropospheric oxidants from photochemical effects of aerosols, *J. Geophys. Res.*, 108(A3), 4097, doi:10.1029/2002JD002622, 2003.

Novelli, P. C., K. A. Masarie, and P. M. Lang, Distributions and recent changes in carbon monoxide in the troposphere, *J. Geophys. Res.*, 103, 19,015–19,033, 1998.

Olivier, J. G. J., A. F. Bouwmann, C. W. M. V. der Mass, J. J. M. Berdowski, C. Veldt, J. P. J. Bloos, A. J. J. Visschedijk, and J. L. Haverlag, Description of EDGAR version 2.0: A set of global emission inventories of greenhouse gases and ozone-depleting substances for all anthropogenic and most natural sources on a per country basis and on $1° \times 1°$ grid, *Tech. Rep. 771060002*, Natl. Inst. of Public Health and the Environ. (RIVM), Bilthoven, Netherlands, 1996.

Palmer, P. I., D. J. Jacob, L. J. Mickley, D. R. Blake, G. W. Sachse, H. E. Fuelberg, and C. M. Kiley, Eastern Asian emissions of anthropogenic halocarbons deduced from aircraft concentration data, *J. Geophys. Res.*, 108, doi:10.1029/2003JD003591, in press, 2003.

Pétron, G., C. Granier, B. Khattatov, J.-F. Lamarque, V. Yudin, J.-F. Müller, and J. Gille, Inverse modeling of carbon monoxide surface emissions using CMDL network observations, *J. Geophys. Res.*, 107(D24), 4761, doi:10.1029/2001JD001305, 2002.

Prather, M., and D. Enhalt, Atmospheric chemistry and greenhouse gases, in *Climate Change 2001: The Scientific Basis*, edited by J. T. Houghton et al., Cambridge Univ. Press, New York, 2001.

Prinn, R. G., et al., Evidence for substantial variation of atmospheric hydroxyl radicals in the past two decades, *Science*, 292, 1882–1888, 2001.

Rodgers, C. D., Retrieval of atmospheric temperature and composition from remote measurements of thermal radiation, *Rev. Geophys. Space Sci.*, *14*, 609–624, 1976.

Rodgers, C. D., *Inverse Methods for Atmospheric Sounding: Theory and Practice*, World Sci., River Edge, N. J., 2000.

Sachse, G. W., G. F. Hill, L. O. Wade, and M. G. Perry, Fast-response, high-precision carbon monoxide sensor using a tunable diode laser absorption technique, *J. Geophys. Res.*, *92*, 2071–2081, 1987.

Singh, H. B., et al., In situ measurements of HCN and CH$_3$CN in the Pacific troposphere: sources, sinks, and comparisons with spectroscopic observations, *J. Geophys. Res.*, *108*(D20), 8795, doi:10.1029/2002JD003006, in press, 2003.

Streets, D. G., et al., An inventory of gaseous and primary aerosol emissions in Asia in the year 2000, *J. Geophys. Res.*, *108*(D21), 8809, doi:10.1029/2002JD003093, in press, 2003.

Stroppiana, D., S. Pinnoch, and J.-M. Gregoire, The Global Fire Product: Daily fire occurrence from April 1992 to December 1993 derived from NOAA AVHRR data, *Int. J. Remote Sens.*, *21*, 1279–1288, 2000.

Tang, Y., et al., Influences of biomass burning during TRACE-P experiment identified by the Regional Chemical Transport Model, *J. Geophys. Res.*, *108*(D21), 8824, doi:10.1029/2002JD003110, in press, 2003.

Yevich, R., and J. A. Logan, An assesment of biofuel use and burning of agricultural waste in the developing world, *Global Biogeochem. Cycles*, *17*, doi:10.1029/2002GB001952, in press, 2003.

Yienger, J. J., M. Galanter, T. A. Holloway, M. J. Phadnis, S. K. Guttikunda, G. R. Carmichael, W. J. Moxim, and H. L. II, The episodic nature of air pollution transports from Asia to North America, *J. Geophys. Res.*, *105*, 26,931–26,945, 2000.
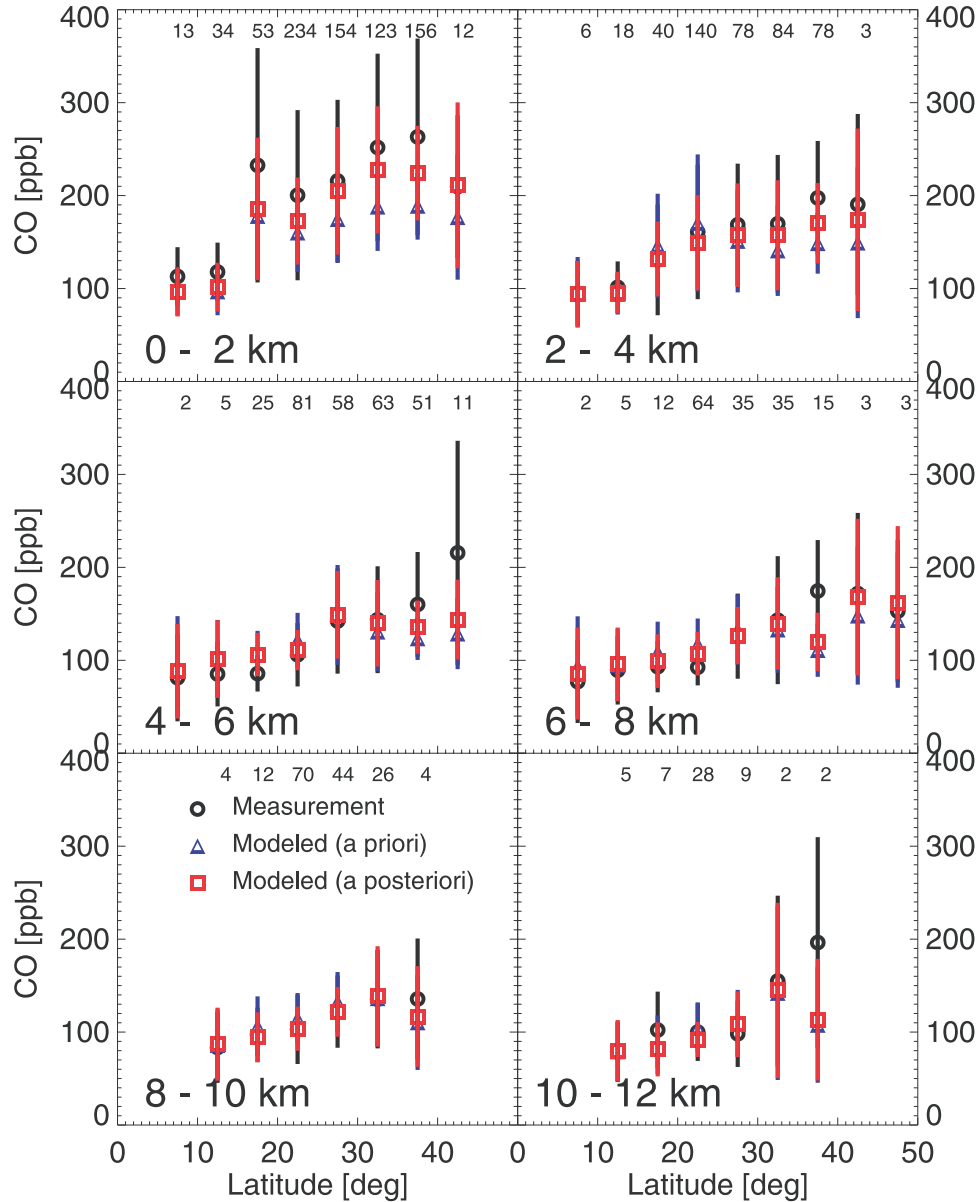
————————————

C. L. Heald, D. J. Jacob, D. B. A. Jones, J. A. Logan, P. I. Palmer, and R. M. Yantosca, Division of Engineering and Applied Sciences, Harvard University, Cambridge, MA 02138, USA. (clh@io.harvard.edu; djj@io.harvard.edu; dbj@io.harvard.edu; jal@io.harvard.edu; pip@io.harvard.edu; bmy@io.harvard.edu)

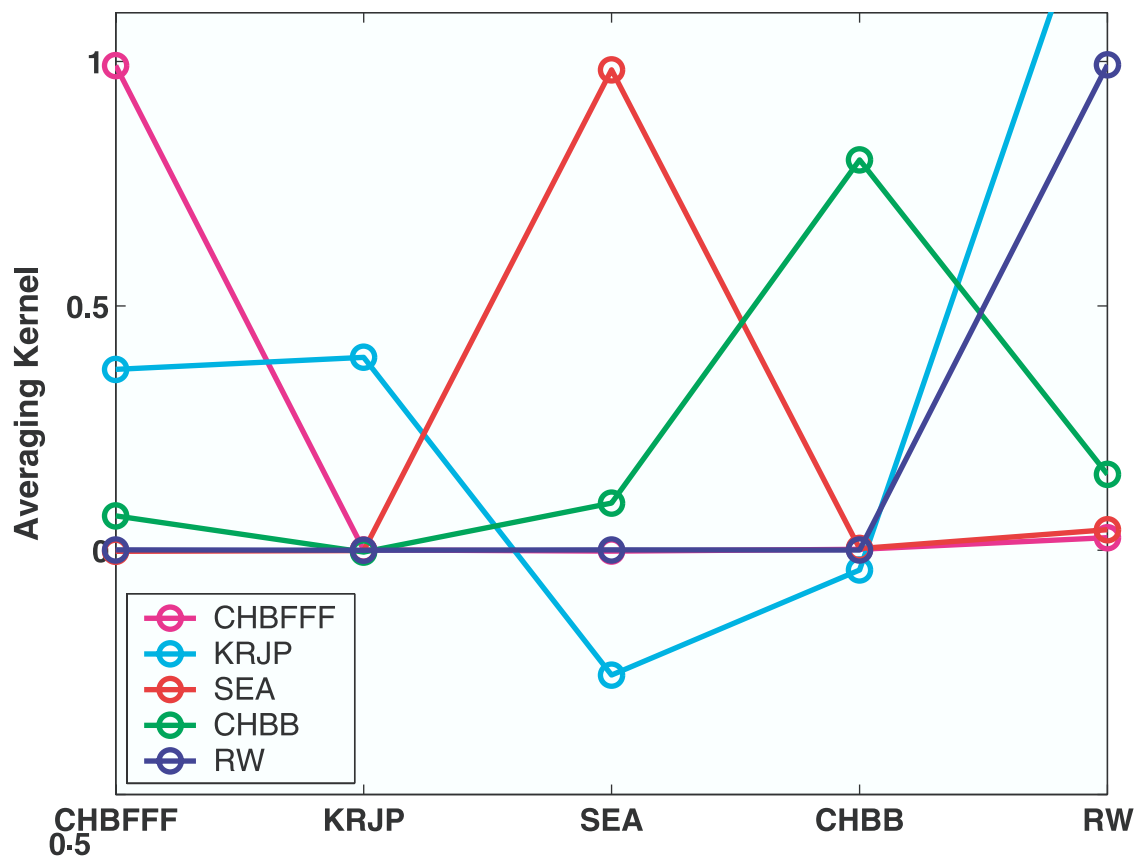G. W. Sachse, NASA Langley Research Center, Hampton, VA 23681, USA. (g.w.sachse@larc.nasa.gov)

D. G. Streets, Argonne National Laboratory, Argonne, IL 60439, USA. (dstreets@anl.gov)
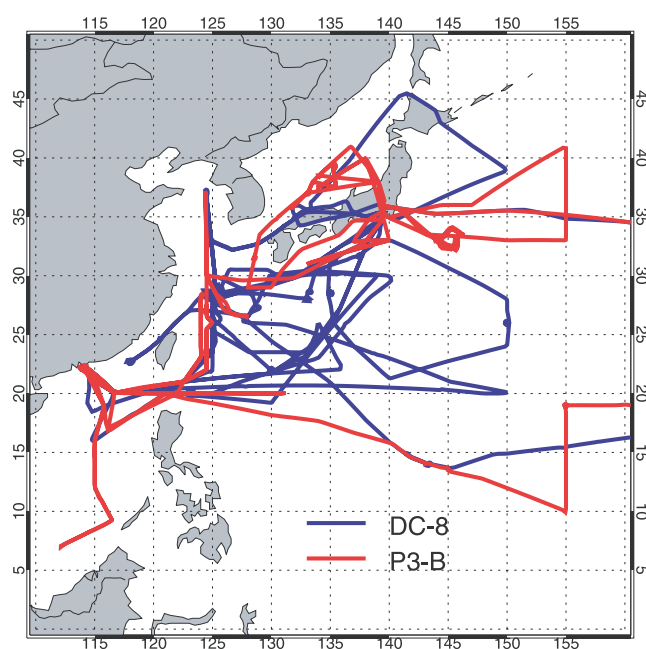
Figure 1. TRACE-P flight tracks for the DC-8 and P3-B aircraft. The inverse model is applied to the ensemble of data west of 150°E which includes 229 hours of CO measurements from the two aircraft, distributed over 28 flights from 27 February to 3 April 2001 [*Jacob et al.*, 2003].
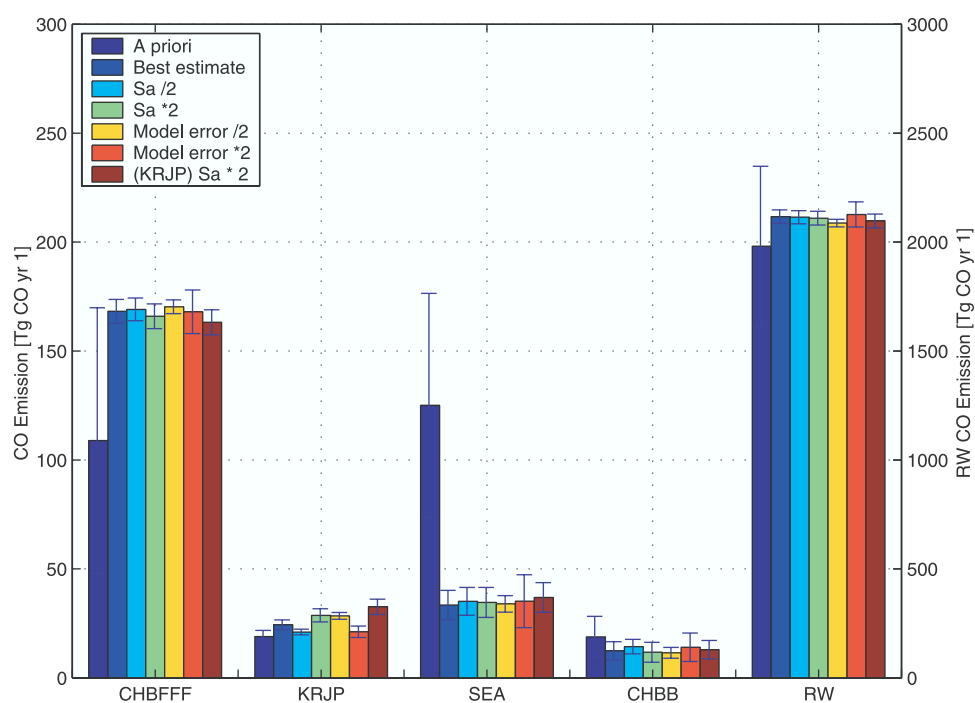
Figure 4. Latitudinal gradients of measured and modeled CO concentrations over the TRACE-P domain on a 2 × 2.5° grid. Observations (circles) are averaged over the altitude range shown in the figure, and over 5° latitude bins. Vertical bars denote 1-σ values about the mean. The model is sampled along the TRACE-P flight tracks for the flight days, and values are averaged across the same latitude and altitude ranges as the observations. Model values are shown for the simulations with a priori (triangles) and a posteriori (squares) sources. Data influenced by the stratosphere ($O_3 > 100$ ppb) or away from the western Pacific rim (longitudes >150°E) have been excluded from the comparison. Numbers inset at the top of each panel refer to the number of observations used to compute the mean statistics.

Figure 6. Individual rows of the averaging kernel matrix **A** for the inversion of CO sources with the TRACE-P observing system. Different colors distinguish rows of **A**, listed in the legend, with the corresponding columns indicated on the x-axis. Lines connect the symbols for clarity and do not have any physical significance. The five-element state vector includes sources from Chinese fuel consumption (CHBFFF), total emissions from Korea and Japan (KRJP), total emissions from Southeast Asia (SEA), Chinese biomass burning (CHBB), and the rest of the world (RW) including the chemical source of CO from the oxidation of CH_4 and biogenic NMVOCs.

Figure 7. Sensitivity of the calculated a posteriori sources to the error estimates in the inverse model. Vertical bars denote 1-σ value from $\hat{\mathbf{S}}$. "Best estimate" shows the a posteriori source from the standard inversion (Table 2). A posteriori sources derived from inversions with modified errors on the a priori source ($\mathbf{S}_a$) or on the model error are also shown. Elements in the abscissa are as in Figure 6.